Impact of Patch Array Antenna Size and Beampattern on Wireless Network Capacity

1st Parmida Geranmayeh
Faculty of Mathematics and Natural Sciences
Department of Computer Science
Humboldt University of Berlin,
Berlin, Germany
Parmida.Geranmayeh@hu-berlin.de

2nd Eckhard Grass
Faculty of Mathematics and Natural Sciences
Department of Computer Science
Humboldt University of Berlin and IHP – Leibniz
Institute for High Performance Microelectronics
Frankfurt (Oder), Germany
grass@ihp-microelectronics.com

Abstract—**Rectangular patch antennas are important components in modern wireless communication systems, including 5G and emerging 6G technologies. These antennas support high-frequency, high-capacity, and energy-efficient wireless communication. For beamforming, the dimensions of these antennas significantly influence their radiation patterns, and antenna gain. Beamforming technology is essential for 5G and 6G networks, enhancing coverage, capacity, and energy efficiency. Effective beamforming relies on array configurations of rectangular patch antennas, with precise control over antenna patterns to improve signal quality and minimize interference.**
This article explores the impact of the size of rectangular patch array antenna in the mmWave frequency band.
The primary goal is to maximize channel capacity between transmitters and receivers. Our study involves simulations using discretized antenna patterns for various patch array antenna sizes, based on realistic room models and a ray-tracing approach. The results demonstrate that larger antenna arrays can significantly increase network capacity. However, selecting the optimal steering vectors for all antennas becomes more complex with increasing antenna size, but is essential for achieving the best configuration.

Keywords— ***Antenna size, Beamforming, Rectangular patch antennas, Wireless network capacity.***

I. INTRODUCTION

In modern wireless communication systems, rectangular patch antennas play a central role, particularly in the context of 5G and emerging 6G networks [1]. These antennas offer advantages such as lightweight construction, compact size, high data rates, high bandwidth, and low power consumption, making them a beneficial choice for 5G wireless communications [2]. Rectangular patch antennas consist of a number of metal patches on a dielectric substrate, typically arranged in a rectangular shape [3]. They function as resonant structures operating at specific frequencies, and are known for their ease of fabrication, and design flexibility [4]. These antennas feature flexible use, low mass, and directional radiation patterns, making them highly suitable for various wireless communication applications [5].

- Sponsor: Deutsche Forschungsgemeinschaft (DFG), Project Number 457407152, Research Project Entitled: 5GEnabled Real Time Communications for Tactile Internet (5G-Remote)

Since the patch size and -spacing is proportional to the wavelength, application of patch array antennas for mmWave and sub-THz systems is very attractive. Smaller patches empower the creation of denser arrays, thereby facilitating precise beamforming and effective interference mitigation [4].

Using patch array antennas with controllable amplitudes and phases for the individual elements with e.g. vector modulators, enables beamforming. This technology within modern wireless systems is instrumental in optimizing signal quality, expanding network capacity, and effectively managing interference [6-10]. The precise control of antenna patterns, facilitates high-quality wireless communication in dynamic and densely populated environments [11,12].

Recent research, such as the adaptive beamforming algorithm outlined in [13] and the innovative flexible beamforming (FBF) architecture introduced by Maheshwari et al. [14], serves as a baseline for the ongoing advancements in beamforming techniques.

This study aims to examine the influence of the rectangular patch array antenna size on the overall channel capacity within a network involving two transmitter-receiver pairs.

The investigation encompasses three distinct antenna sizes, namely 4×4, 4×8, and 4×16, in order to assess the performance variations associated with these dimensions. These sizes define the spatial configuration of the antenna array, indicating the number of antenna elements in both the vertical and horizontal directions. The reason for choosing these sizes is their availability for experimental verification, and the fact that steerability in the horizontal direction is typically more important than in the vertical direction. Based on complex simulation models, we seek to gain insights into the impact of antenna size on the network's total channel capacity.

II. IMPLEMENTATION

In this section, we elaborate on the fundamental aspects of our implementation, which entail an exhaustive search

procedure comprising 923,521 iterations for each of the three antenna sizes: 4×4, 4×8, and 4×16. These iterations are derived from the range of the steering vectors, horizontally spanning -45 to +45 degrees, with a 3-degree step, resulting in 31 values per antenna. This leads to a total of 31×31×31×31=923,521 unique combinations. For each combination, the total channel capacity is calculated, with the goal of identifying the configuration that yields the highest capacity. For this purpose, 1st order reflections are taken into account, and interference of radiated energy from sidelobes of the antenna pattern is estimated. Based on the received (desired) signal of each receiver and the received (undesired) interference, the signal to noise plus interference ratio (SNIR) and subsequently the channel capacity for each beam configuration is calculated [15].

Fig. 1 illustrates our room model and visualization in MATLAB, where we use an STL file named `office.stl` to represent a 3D room model. This model is rendered using the `siteviewer` function with the `SceneModel` option. This facilitates the exploration of a room measuring 8m in length, 5m in width, and 2.75m in height. Our simulated communication system operates at a 60 GHz carrier frequency, with a fixed bandwidth of 2 GHz and employs 4 antennas, considering a range of horizontal angles spanning -45 to 45 degrees for each antenna. The material of the room is concrete. Using a frequency of 60 GHz and a bandwidth of ca. 2 GHz in an indoor environment comes with several advantages and considerations. The 60 GHz frequency, e.g. standardized in IEEE802.11ad falls within the mmWave spectrum, which is a range of frequencies above 24 GHz. The short wavelength enables the design of patch array antennas of small formfactor and yet high gain. mmWave frequencies offer a large amount of available spectrum, which is beneficial for accommodating the growing demand for wireless data. The 2 GHz bandwidth provides ample capacity for supporting high data rates.

It's important to note that the setup we're discussing here doesn't involve any unique or specific room conditions. We've opted for a general room setup and layout with a generalized configuration. Additionally, the choice of antenna locations isn't tied to any particular scenario. As a result, we anticipate that the conclusions drawn won't be affected even if we were to alter the rooms and locations of the antennas. Even though the findings apply to the specific room used, we assume that the results will be similar across different setups.

The Uniform Rectangular Array antennas (URA) are modelled using the `phased.URA` function, with configurations for three conditions: 4 rows and 4 columns with half-wavelength spacing for the first condition, 4 rows and 8 columns with half-wavelength spacing for the second condition, and 4 rows and 16 columns with half-wavelength spacing for the third condition. The positions of the receiver (Rx) and transmitter (Tx) are chosen as follows:

Tx_1: (0.02, 8, 2)

Tx_2: (5, 8, 2)

Rx_1: (4.5, 3.5, 0.85)

Rx_2: (2, 4, 0.85)

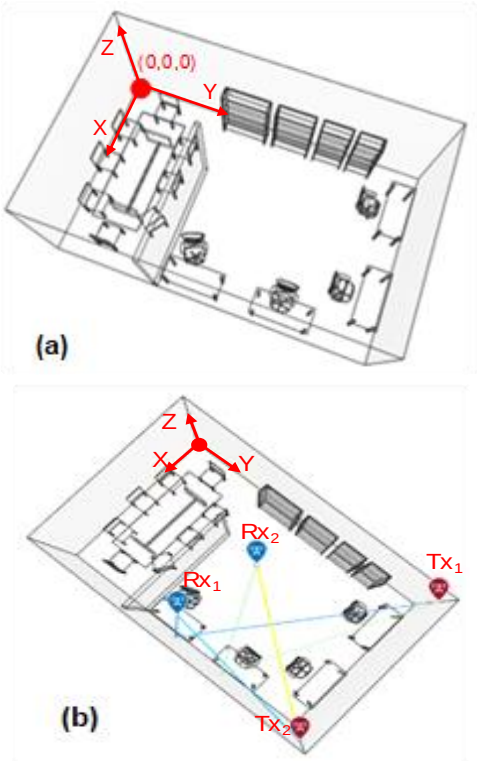

Fig. 1. (a) The room layout model. **(b)** The antennas placement in the model room.

In our implementation, we establish a `ray-tracing` propagation model within a Cartesian coordinate system, utilizing the shooting and bouncing ray method (SBR) with low angular separation. This model focuses on evaluating the channel capacity across a wide range of transmitter (Tx) and receiver (Rx) angles. Our implementation involves a substantial number of 923,521 combinations using nested loops to explore all Tx and Rx angles. Within the loops, we use MATLAB's Phased Array System Toolbox to calculate antenna patterns for different Tx and Rx steering vectors. This process includes creating a steering vector, defining desired scan angles, calculating beamforming weights, and using the pattern function to derive radiation patterns. These patterns depend on the design and characteristics of the antenna elements, with the `patchMicrostrip` and `phased.CosineAntennaElement` classes, facilitating beamforming. Custom antenna models are generated based on these patterns and specified azimuth and elevation angles, leading to the creation of transmitter (`tx`) and receiver (`rx`) objects.

The number of bits used in the discretized antenna patterns is 64 bits (for gain), providing high precision, a wide dynamic range for accurate representation, and computational efficiency. With a 64-bit resolution and an angular step-size of 3 degrees, the representation can accurately capture subtle variations in gain across different angles. Additionally, the wide dynamic range ensures that the diverse gain values exhibited by antenna patterns are represented without compromising precision. This choice aligns with industry standards and supports compatibility with numerical tools.

The `ray-trace` function is employed to perform ray tracing, including path loss, path phase, angle of departure (AoD), and angle of arrival (AoA). These values are processed through transformation matrices to convert global spherical coordinates to local spherical coordinates. The antenna patterns for each transmitter and receiver configuration, e.g. as depicted in Fig. 2, are then computed using the "pattern" function. Path gains are computed by combining antenna patterns with path characteristics and subsequently matched with corresponding path delays. In this implementation, the calculation of path gains and receive-power involves the utilization of antenna patterns, path loss, and phase information. Specifically, the transmit antenna pattern (`patTx`) is determined using the `pattern` function applied to azimuth and elevation angles (`AoD`) for the specified transmitter index (`TxIndex`). Similarly, the receive antenna pattern (`patRx`) is calculated for the designated receiver index (`RxIndex`) using the `pattern` function and azimuth and elevation angles (`AoA`). The resulting arrays, `patTx` and `patRx`, contain the transmit and receive antenna pattern values for each corresponding angle pair.

The subsequent step involves the computation of path gains (`pathGains`) using the calculated antenna patterns, along with the provided path loss (`pathLoss`) and phase information (`pathPhase`). Equation (1) represents the power term, determining signal magnitude. Equation (2) specifies the phase term, affecting signal phase. `pathGains` is the resulting complex-valued array with calculated gains for each angle pair.

$$P = 10^{(patTx - pathloss + patRx)/20} \quad [16] \tag{1}$$

$$PathPhase = e^{(1i \times pathPhase)} \quad [16] \tag{2}$$

To quantify the total receive power for each device (transmitter-receiver beam pair), the coefficients of the path gains for all rays are summed using the `sum` function, and the result is stored in the matrix `TotalPower_per_device($Tx_{Index}$, $Rx_{Index}$)`. This step provides insight into the cumulative power associated with the communication link between the specified transmitter and receiver.

The process encompasses all rays, concluding with the calculation of total power received by each device and the channel capacity assessment for every transmitter-receiver beam pair. These channel capacity values are then stored in the `ChannelCapacity$Tx_1Rx_1$`, `ChannelCapacity$Tx_2Rx_2$` and `Total_Channel_Capacity` arrays for further analysis. (Equations 1-3)

$$SINR = (Signal\ Power) / (Interference\ Power + Noise\ Power) \quad [14] \tag{3}$$

$$C_{channel\ capacity} = B \times log_2(1+SINR) \quad [14] \tag{4}$$

$$C_{Total\ channel\ capacity} = Channel\ capacity_{\ TX1RX1} + Channel\ capacity_{\ TX2RX2} \tag{5}$$

In this formula, `C` represents the channel capacity in bps, `B` denotes the channel's bandwidth in hertz (Hz), and `SINR` is the Signal-to-Interference-plus-Noise Ratio.

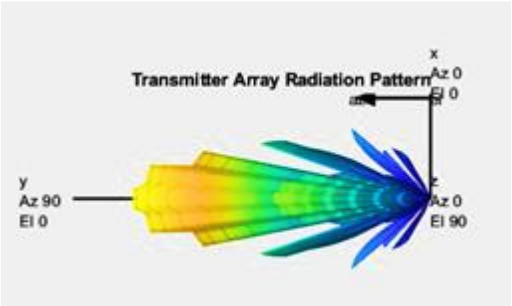

Fig. 2. The digitized antenna radiation pattern.

The simulation runs through all possible combinations of transmitter and receiver steering vectors and, hence, allows identifying the optimal configuration that maximizes the total channel capacity across all nodes. This process is carried out for all three antenna sizes, and the results are compared in the next section.

III. RESULTS AND DISCUSSIONS

Fig. 3 illustrates the maximum total channel capacity that has been achieved for each antenna size. The total transmit power was constant for all three configurations at 500mW. As depicted in the figure, the 4×16 antenna configuration has attained the highest total channel capacity, reaching a value of 51.3 Gbps, with the steering vectors in degrees (T_{X1}=-30, T_{X2}= -36, R_{X1}=36, R_{X2}=30). Following that, the 4×8 antenna has achieved a total channel capacity of 39.1 Gbps with the steering vectors (Tx1=-39, Tx2=-45, R_{X1}=45, Rx2=39), and the 4×4 antenna has achieved a total channel capacity of 31.5 Gbps with the steering vectors (T_{X1}=39, T_{X2}=-42, Rx1=-33, R_{X2}=45), occupying the lowest position among the configurations. This order underscores the relationship between antenna size and channel capacity, wherein larger antennas generally result in larger gain and, hence, channel capacity.

Fig. 4 presents the average channel capacity across all three antenna sizes. The average channel capacity is determined by dividing the total channel capacity summed across all beam configurations by the total number of beam configurations, which is 923,521. The results indicate that the 4×4 antenna exhibits the highest average channel capacity, at approximately 13.6 Gbps. Following this, the 4×16 antenna achieves an average of 6.34 Gbps, and the 4×8 antenna follows closely with an average of 4.77 Gbps. Despite the 4×16 antenna providing the maximum total channel capacity, the 4×4 antenna outperforms in terms of the average total channel capacity values. The 4×4 antenna exhibits a wider radiation pattern with less pronounced variation of gain in specific directions, enhancing its ability to establish effective communication with transmitter-receiver pairs, even if a non-optimal steering vector is chosen. Conversely, larger antennas, such as 4×8 and 4×16 configurations, are more sensitive to choosing the optimum steering vectors due to their narrower radiation patterns.

Consequently, the average total channel capacity of a 4×4 antenna surpasses that of its larger counterparts. Interestingly, the diagram of average channel capacity against antenna size in Fig. 4 does not show monotonicity. This is probably due to a second effect related to the interference. The smaller the antenna size and the broader the beam, the higher the probability of interference becomes. As a consequence, the 4×8 antenna shows the smallest average channel capacity.

Fig. 5 illustrates the maximum standard deviation values across different antenna sizes, representing the variations in channel capacity. The 4×16 antenna size exhibits the highest standard deviation at approximately 5.91 Gbps, indicating greater fluctuations in capacity values. Following this, the 4×4 antenna size shows a standard deviation of around 4.44 Gbps. In contrast, the 4×8 antenna size displays a lower standard deviation of approximately 3.9 Gbps, reflecting relatively stable capacity values for this configuration. For the non-monotonic characteristic, a similar reasoning as for the average channel capacity applies.

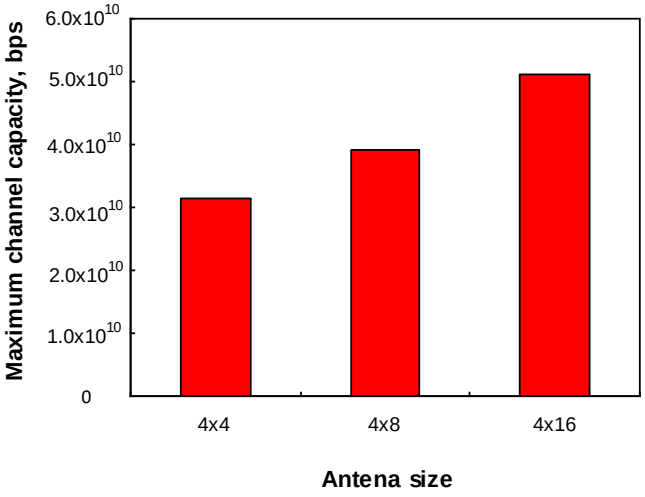

Fig. 3. Antenna size vs. maximum channel capacity.

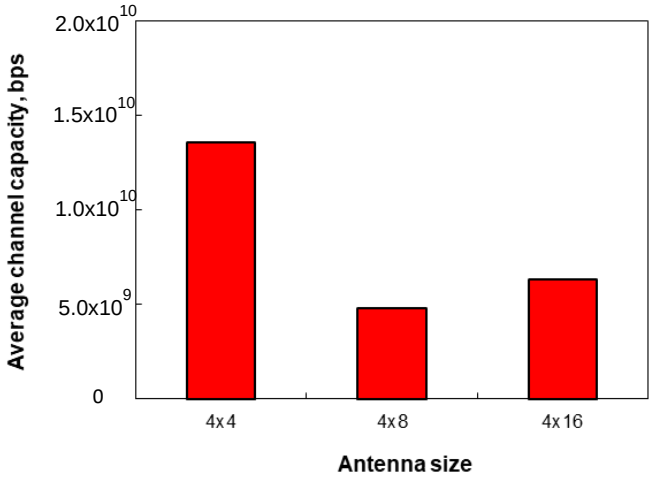

Fig. 4. Average channel capacity across different antenna sizes.

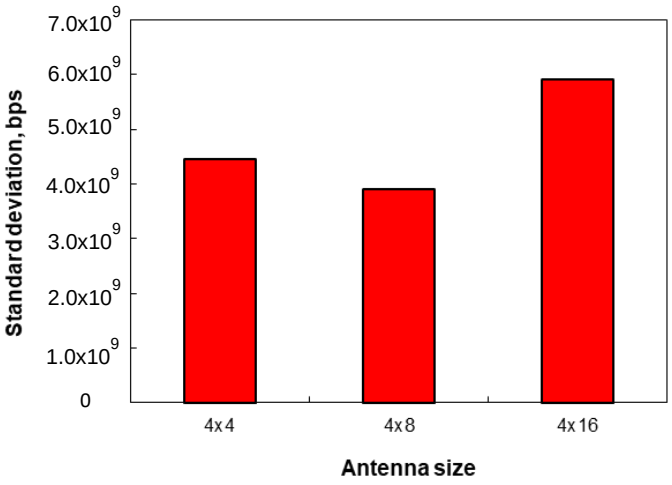

Fig. 5. Maximum standard deviation values across different antenna sizes.

Fig. 6 presents histograms of the channel capacity values across the three distinct antenna sizes. This graphical representation not only elucidates the range of average channel capacity for each antenna size but also highlights their distribution. As expected, for the 4×4 antenna, the channel capacity is spread over a large range with a large average value. For the larger antennas, the average is smaller with many calculated channel capacities in the very small range. This analysis enhances our understanding of the statistical properties and performance characteristics of the communication system under investigation.

As observed in the figure, the antenna with dimensions 4×16 exhibits the highest total channel capacity, while the average capacity of the 4×4 antenna surpasses that of the other antennas. In the 4×16 configuration, the curve exhibits a sharper peak, and a relatively large number of results fall within the high-value range. In contrast, the 4×4 configuration yield a broad distribution with results spanning a wide range. Moreover, it is noteworthy that the 4×8 antenna demonstrates a comparatively lower data diversity. The difference in the diversity of total channel capacity between the 4×4, 4×8 and 4×16 antennas is primarily due to their distinct radiation patterns. The 4×16 antenna focusses in specific directions, leading to a denser concentration of data rates in those areas, while the 4×4 antenna, with its broader pattern, spreads data rates, resulting in a broader distribution. This detailed examination of channel capacity variations among different antenna sizes is crucial for optimizing communication system performance, beam training and resource allocation strategies.

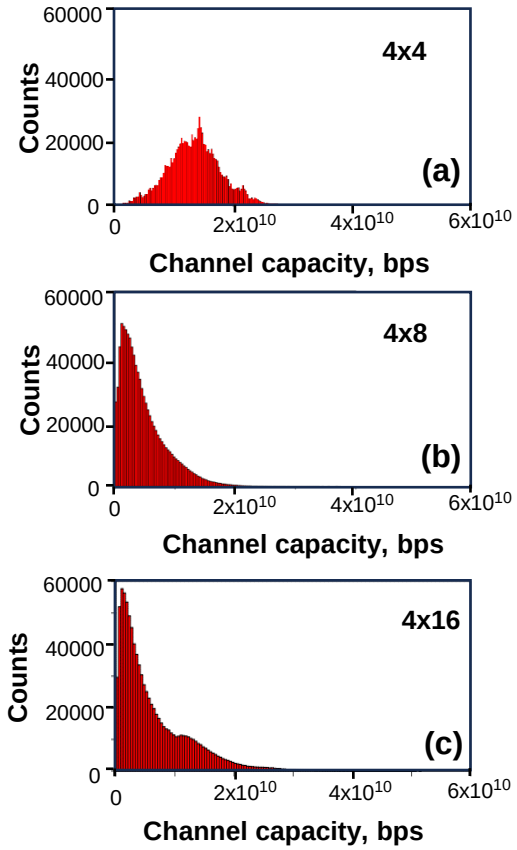

Fig. 6. Histogram of channel capacity distribution across three antenna sizes.

IV. CONCLUSION

In this article, we investigate the role of the size of rectangular patch antennas in mmWave wireless communication systems. We conducted a comparative analysis of the total channel capacity with beamforming technology for three different antenna sizes. The results indicate that the 4×16 antenna configuration achieves the highest total channel capacity, while the 4×4 antenna provides a good average capacity, despite its smaller size. Our quantitative exploration underscores the significance of understanding channel capacity variations among different antenna sizes. This can be vital for optimizing system performance, beam training and resource allocation. It is shown, that deployment of the largest antenna yields the highest maximum channel capacity. On the other hand, the statistical data indicates, that smaller antennas are less sensitive to identifying, applying and maintaining the optimum beam configuration in a wireless network.

ACKNOWLEDGMENT

The authors thank the Deutsche Forschungsgemeinschaft (DFG), Project number 457407152, for providing financial support of the research project entitled “5GEnabled Real Time Communications for "Tactile Internet" (5G-Remote)”.

REFERENCES

[1] P. Bhartia, I. Bahl , and R. Garg. “Microstrip antenna design handbook (Artech house antennas and propagation library)”, Artech house publishers, 2000, ISBN: 978-0890065136.

[2] C.A. Balanis “Antenna theory: analysis and design”, Wiley-interscience, 4th Edition, 2016, ISBN: 0-471-66782-X.

[3] D.M. Pozar, “Microstrip antennas”, Proceedings of the IEEE, Vol.80, no.1, pp. 79-91, 1992, DOI: 10.1109/5.119568.

[4] Y. Rahmat-Samii, and E. Michielssen ., “Electromagnetic optimization by genetic algorithms”, Wiley-interscience, 1st Edition, 1999, ISBN: 978-0471295457.

[5] N.A. Muhammad, Y.M. Muhammad, Y. Idris, A.B. Kunya, “Design and analysis of rectangular microstrip patch antenna resonating at 5.2GHz for WLAN applications”, Int. Conf. Elec. Eng. App., 2020.

[6] R.W. Bickmore, “Adaptive antenna arrays”, IEEE spectrum, pp. 78-88, 1964.

[7] W. He, C. Zhang, J. Deng, Q. Zheng, Y. Huang, and X. You, “Conditional generative adversarial network aided digital twin network modeling for massive MIMO optimization”, IEEE Wireless communications and networking conference (WCNC), 2023, DOI: 10.1109/WCNC55385.2023.10118756.

[8] J. Jalali, A. Khalili, A. Rezaei, J. Famaey, and W. Saad, “Power-efficient antenna switching and beamforming design for multi-user SWIPT with non-linear energy harvesting”, IEEE 20th consumer communications & networking conference (CCNC), 2023, DOI: 10.1109/CCNC51644.2023.10059879.

[9] G. Charis, and N. showme, “Beamforming in wireless communication standard: A survey”, Indian journal of science and technology, Vol. 10, 2017.

[10] B. Salehi, Utku Demir, D. Roy, S. Pradhan, J. Dy, S. Ioannidis, and K. Chowdhury, “Multiverse at the edge: interacting real world and digital twins for wireless beamforming”, 2023, DOI: 10.48550/arXiv.2305.10350.

[11] N. Ojaroudi-Parchin, Y.I.A. Al-Yasir, R. Abd-Alhameed, M. Ahmed, Abdulkhaleq, and J.M. Noras, “Recent developments of reconfigurable antennas for current and future wireless communication systems”, 2019, DOI: 10.3390/electronics8020128.

[12] S. Mikki, “The antenna spacetime system theory of wireless communications”, Proceeding of the royal society A, 2018, DOI: 10.1098/rspa.2018.0699.

[13] C.K. Kim, “Performance improvement of MIMO-OFDMA system with beamformer”, 2019, DOI: 10.7236/IJIBC.2019.11.1.60.

[14] M.K. Maheshwari, M. Agiwal, N. Saxena, And A. Roy, “Flexible beamforming in 5G wireless for internet of things”, IETE technical review, Vol. 36, no. 1, 2019.

[15] J. G. Proakis, and M. Salehi, “Digital Communication”, McGrow-hill, 5th edition, 2008, ISBN 978–0–07–295716–7.

[16] K. Sinan, and T. Bulent, “Path-loss modeling for wireless sensor networks: A review of models and comparative evaluations”, IEEE Antennas Propag. Mag., Vol. 59, No. 1, pp. 18-37, 2017, DOI: 10.1109/MAP.2016.2630035.